Contrib Mineral Petrol (2014) 167:981
DOI 10.1007/s00410-014-0981-y

ORIGINAL PAPER

Komsomolskaya diamondiferous eclogites: evidence for oceanic crustal protoliths

John F. Pernet-Fisher · Geoffrey H. Howarth · Yang Liu · Peter H. Barry · Laura Carmody · John W. Valley · Robert J. Bodnar · Zdislav V. Spetsius · Lawrence A. Taylor

Received: 24 October 2013 / Accepted: 3 February 2014 / Published online: 18 February 2014

Abstract The Komsomolskaya kimberlite is one of numerous (>1,000) kimberlite pipes that host eclogite xenoliths on the Siberian craton. Eclogite xenoliths from the adjacent Udachnaya kimberlite pipe have previously been geochemically well characterized; however, data from surrounding diamond-bearing kimberlite pipes from the center of the craton are relatively sparse. Here, we report major- and trace-element data, as well as oxygen isotope systematics, for mineral separates of diamondiferous eclogite xenoliths from the Komsomolskaya kimberlite, suggesting two distinct subgroups of a metamorphosed, subducted oceanic crustal protolith. Using almandine contents, this suite can be divided into two subgroups: group B1, with a high almandine component (>20 mol%) and group B2, with a low almandine component (<20 mol%). Reconstructed REE profiles for B1 eclogites overlap with typical oceanic basalts and lack distinct Eu anomalies. In addition, elevated oxygen isotope values, which are interpreted to reflect isotopic exchange with seawater at low temperatures (<350 °C), are consistent with an upper-oceanic crustal protolith. Reconstructed REE profiles for B2 eclogites are consistent with oceanic gabbros and display distinct Eu anomalies, suggesting a plagioclase-rich cumulate protolith. In contrast to B1, B2 eclogites do not display elevated oxygen isotope values, suggesting an origin deep within the crustal pile, where little-to-no interaction with hydrothermal fluids has occurred. Major-element systematics were reconstructed based on mineral modes; group B1 eclogites have higher MgO wt% and lower SiO_2 wt%, with respect to typical oceanic basalts, reflecting a partial melting event during slab subduction. Calculated residues from batch partial melt modeling of a range of Precambrian basalts overlap with group B1 trace-element chemistry. When taken together with the respective partial melt trajectories, these melting events are clearly linked to the formation of Tonalite–Trondhjemite–Granodiorite (TTG) complexes. As a result, we propose that many, if not all, diamondiferous eclogite xenoliths from Komsomolskaya represent mantle 'restites' that preserve chemical signatures of Precambrian oceanic crust.

Keywords SCLM · Eclogites · Siberian craton · Mantle xenolith · TTG complex

Communicated by T. L. Grove.

J. F. Pernet-Fisher (✉) · G. H. Howarth · Y. Liu · P. H. Barry · L. Carmody · L. A. Taylor
Department of Earth and Planetary Sciences, Planetary Geosciences Institute, University of Tennessee, Knoxville, TN 37996, USA
e-mail: jpf@utk.edu

Y. Liu
Jet Propulsion Laboratory, California Institute of Technology, Pasadena, CA 91109, USA

J. W. Valley
Department of Geoscience, University of Wisconsin, Madison, WI 53706, USA

R. J. Bodnar
Department of Geosciences, Virginia Polytechnic and State University, Blacksburg, VA 24061, USA

Z. V. Spetsius
Institute of Diamond Industry, ALROSA Company, Ltd., Mirny, Yakutia, Russia

Introduction

Eclogites make up a minor (<2 %), but important, component in mantle xenolith suites and are transported to the surface by kimberlite magmas; as such, these eclogites

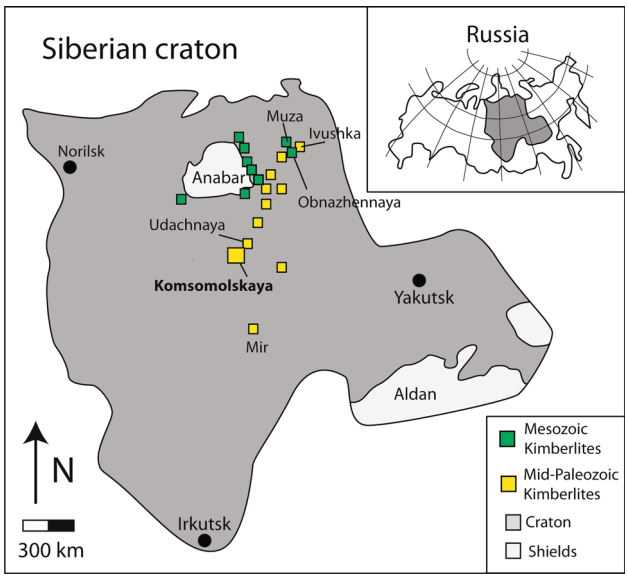

Fig. 1 Simplified geological map of the Siberian craton showing regional distribution of Mesozoic and Mid-Paleozoic Kimberlite pipes

represent one of the main diamond reservoirs on Earth. Siberian eclogite xenoliths have generally been interpreted to represent sections of recycled oceanic crust (e.g., Taylor and Neal 1989; Jacob et al. 1994; Beard et al. 1996; Snyder et al. 1997). Typical lines of evidence for this interpretation include (1) non-mantle-like oxygen isotope ratios, which are generally considered to be robust against metamorphic, and subduction-induced fractionation (e.g., Eiler 2001); (2) reconstructed bulk-rock, trace-element concentrations, which can also be used to exclude the effects of metasomatism (e.g., Taylor and Neal 1989; Jacob et al. 2009); and (3) the preservation of mass-independent sulfur isotope fractionation within diamond sulfide inclusions in eclogites that relate to the recycling of sedimentary materials associated with these rocks (e.g., Farquhar et al. 2002). Taken together, these lines of evidence strongly indicate a low-pressure origin for the eclogite protolith; however, this interpretation is not universally accepted. An alternative origin as intrusive high-pressure magmatic cumulates within the mantle has also been proposed (Hill and Haggerty 1989; Caporuscio and Smyth 1990; Griffin and O'Reilly 2007), suggesting that extreme metasomatic processes, such as the oxidization of methane-rich fluids, are able to account for non-mantle oxygen isotope variations and measured bulk-rock systematics (e.g., Griffin and O'Reilly 2007). Deciphering which hypothesis is valid is critical, as these rare xenoliths can potentially provide a unique perspective into Precambrian oceanic crustal lithologies and tectonics.

Here, we present major- and trace-element data along with oxygen isotope ratios of Komsomolskaya garnet and clinopyroxene mineral separates. Samples were selected from a suite of 16 diamondiferous eclogite xenoliths of the Late Devonian Komsomolskaya pipe. This pipe is located in the center of the Siberian craton, within the Alakit kimberlite field, near the well-characterized Udachnaya pipe (Fig. 1; Davis et al. 1980; Kharkiv et al. 1998). Siberian eclogites have previously been dated to ~2.7–2.9 Ga, using Re–Os and Pb–Pb techniques (Jacob et al. 1994; Pearson et al. 1995). The aim of this study is to geochemically characterize Komsomolskaya samples, in the context of other Siberian Craton eclogites, in order to place robust constraints on the origin of eclogites within the Siberian subcontinental lithospheric mantle (SCLM).

Methods

Fresh garnet and clinopyroxene grains were picked from 16 crushed diamondiferous eclogite xenoliths. Samples were cleaned in an ultrasonic bath for 30 min each at room temperature, using concentrated hydrochloric acid followed by acetone. From each set of mineral separates, 1–4 pristine grains from the 1- to 500-μm-size and 250- to 500-μm-size fractions were selected for major-, minor-, and trace-element analysis. Several grains were selected when mineral separates displayed significant color variations. The minerals were mounted in epoxy and polished in preparation for analysis.

Major-element compositions were measured using a CAMECA SX-100 electron microprobe (EMP) at the University of Tennessee. Garnet and clinopyroxene compositions were collected using a 10-μm-beam size, a 20-nA-beam current, and an accelerating voltage of 15 kV. Counting times for each element were generally 20 s, except for Cr (40 s), Ni (60 s), and P (60 s). Standard PAP (ZAF) corrections were applied to all analyses. Detection limits were: <0.03 wt% for SiO_2, TiO_2, Al_2O_3, MgO, CaO, Na_2O, and K_2O; and <0.05 wt% for MnO, FeO, Cr_2O_3, NiO, and P_2O_5.

Minor- and trace-element analyses were performed on the same garnet and clinopyroxene crystals as were the major-element analyses, using a GeoLas Pro (193 nm) laser-ablation system coupled to an Agilent 7,500 ce inductively coupled plasma mass spectrometer (ICPMS) at Virginia Polytechnic and State University. Samples were analyzed with a 60-μm spot, with a repetition rate of 5 Hz for a minimum of 60 s, with a preliminary 10 s for stabilization/equilibration prior to inlet into the mass spectrometer. A photon fluence rate of 7–10 J/cm^2 was employed for each sample. Data were acquired for ^{45}Sc, ^{49}Ti, ^{62}Ni, ^{88}Sr, ^{89}Y, ^{90}Zr, ^{93}Nb, ^{139}La, ^{140}Ce, ^{141}Pr, ^{143}Nd, ^{147}Sm, ^{153}Eu, ^{157}Gd, ^{159}Tb, ^{163}Dy, ^{165}Ho, ^{166}Er, ^{169}Tm, ^{172}Yb, ^{175}Lu, and ^{178}Hf. The NIST 610 glass standard was

used for machine calibration, and an internal standard, using the concentration of Ca obtained from the EMP analysis, was used to check reproducibility, with values generally within the analytical uncertainty (1 σ) of the EMP value. Two analyses of the NIST 610 standard were completed before and after each sample analysis to correct for machine drift. Detection limits of trace-elements vary from 10 to 200 ppb, depending on sample and ablation time. Minor- and trace-element precision of the standard was approximately 3 % (RSD) or better, and accuracy was within 2 σ of the reported values, with an average error of 5–15 %.

Oxygen isotopes were measured, at the University of Wisconsin, Madison, on garnet separates using laser fluorination and gas source mass spectrometry. Prior to analysis, the samples were cleaned with isopropanol and methylene chloride, to remove any contaminants. The oxygen isotope analyses were performed on garnet mineral separates, approximately 1–2 mg per run, using a 32 W CO_2 laser, BrF_5, and a dual-inlet Finnigan MAT 251 mass spectrometer (Valley et al. 1995). All $\delta^{18}O$ values are reported with respect to Vienna—Standard Mean Ocean Water (V–SMOW). During analytical runs, the garnet standard UWG-2 yielded a mean $\delta^{18}O$ value of 5.77 ± 0.14 ‰ (2σ), and $\delta^{18}O$ values were corrected to the recommended value of 5.80 ‰ V-SMOW (Valley et al. 1995). Replicate analyses were performed on several samples, including those that had initial oxygen isotope values outside of the normal mantle range of 4.7–5.9 ‰ (Mattey et al. 1994; Valley 2003).

Results

Garnet

Garnet compositions are characterized by low Cr_2O_3 contents (<1.2 wt%), but variable CaO (3–17 wt%) and FeO (9–18 wt%) concentrations (Table 1). Several classification schemes have been devised for garnet based on major-element concentrations (Coleman et al. 1965; Sobolev et al. 1973; MaCandless and Gurney 1989; Taylor and Neal 1989; Grutter et al. 2004). Here, we adopt the scheme developed by Coleman et al. (1965) and modified by Taylor and Neal (1989), based on relative pyrope, almandine, and grossular proportions, as this classification has been widely used for Siberian eclogites (Fig. 2). All garnets in this study plot within group B of this classification scheme. Based on almandine content, this suite can be further divided into two subgroups: group B1 with a high almandine component (>20 mol%) and group B2 with a low almandine component (<20 mol%). Several garnets were analyzed per sample and generally plot within the same groupings; however, a small number of samples contain mixed populations of group B1 and B2 garnets (e.g., sample K9, K14). Notably, similar subgroups based on almandine components have been observed from eclogites worldwide (e.g., Jacob and Foley 1999; Aulbach et al. 2007; Riches et al. 2010).

Group B1 garnets are generally characterized by Cr_2O_3 extending up to ~1.2 wt% at a near-constant CaO of ~3 wt% and FeO contents >17 wt%; in contrast, K14 has higher CaO (6.7 wt%) and lower FeO (16.4 wt%), with respect to other B1 eclogites. All B1 samples have strong negative Ti anomalies, relatively high HREE concentrations (up to 30 × chondrite), and lack Eu anomalies (Fig. 3a, c). Group B2 garnets are characterized by Cr_2O_3 < 0.2 wt% and variable CaO ranging up to 18 wt%, as well as low Na_2O (<0.1 wt%), and minor negative Ti anomalies. Concentrations of HREEs range from chondritic up to 5× chondrite (Fig. 3b, d). The MREEs are typically more enriched than the HREEs, resulting in a negative MREE–HREE slope. Generally, this group has moderate positive Eu anomalies, ranging from Eu/Eu* 1.39 to 2.01 (Fig. 4).

Oxygen isotope ratios

Oxygen isotope ($\delta^{18}O$) ratios were measured on garnet separates (Table 1). As with the mineral major- and trace-element chemistry, $\delta^{18}O$ values display distinct differences between the B1 and B2 groupings (Figs. 5, 6). The B1 garnet $\delta^{18}O$ values extend from 6.2 to 8.1 ‰, falling above the average mantle range (4.7–5.9 ‰; Mattey et al. 1994; Valley 2003). In contrast, group B2 garnets have a more restricted range of $\delta^{18}O$, varying from just 5.3–5.5 ‰, overlapping the mantle range.

Clinopyroxene

Clinopyroxenes contain between 25–48 mol% jadeite component, classifying them as omphacite. The Taylor and Neal (1989) 'A-B-C' classification can also be applied to clinopyroxenes based on their MgO and Na_2O concentrations (Table 2, Fig. 2b). The majority of samples are consistent with divisions observed from the garnet classification, falling largely within group B. However, two clinopyroxenes plot significantly outside of the group B field, instead plotting within the group A field (Fig. 2b). Some samples show mixed populations; e.g., K1 and K12 contain both group A and B clinopyroxenes.

With consideration of trace elements, systematic REE and trace-element differences are also observed in the clinopyroxenes, corresponding to the B1 and B2 subdivisions (Fig. 4). B1 clinopyroxenes have higher REE concentrations than B2 clinopyroxenes and show enrichments in LREE–MREE, displaying a 'humped' REE profile with

Table 1 Major-, trace-element, and oxygen isotope data for Komsomolskaya garnets; n/a = not analyzed

Group	K1a B1	K1b B1	K9b B1	K10 B1	K14a B1	K15a B1	K16 B1	K2a B2	K2b B2	K3 B2	K4 B2	K5a B2	K5b B2	K6 B2	K7 B2	K8 B2	K9 B2	K11 B2	K12 B2	K13 B2	K14b B2
SiO_2 (wt%)	40.9	40.9	40.7	40.8	39.9	40.5	40.7	40.5	40.8	40.7	40.4	40.6	39.7	40.6	40.2	40.7	40.2	41	41.3	40.9	41.6
TiO_2	0.31	0.25	0.27	0.27	0.47	0.28	0.21	0.14	0.11	0.11	0.14	0.23	0.23	0.12	0.33	0.11	0.34	0.11	0.08	0.08	0.09
Al_2O_3	22.0	22.2	21.9	22.3	22.0	21.7	22.1	22.7	23.0	23.0	22.7	22.6	22.0	22.8	22.6	22.9	22.6	23.0	23.0	23.0	23.3
FeO	17.4	17.9	17.3	17.2	18.4	16.4	17.6	11.3	10.7	9.1	11.3	11.7	11.3	9.61	9.88	10.1	10	10.1	10.8	10.2	10.1
MnO	0.29	0.30	0.29	0.29	0.40	0.28	0.31	0.24	0.22	0.17	0.24	0.23	0.22	0.20	0.18	0.19	0.18	0.20	0.21	0.21	0.21
CaO	3.8	3.2	3.4	3.3	6.7	4.0	2.7	13.8	12.1	15.4	13.7	14.2	14.1	15.8	16.8	12.6	16.9	12.4	7.8	10.9	10.7
MgO	15.5	15.6	15.6	15.8	11.9	15.3	16.0	11.4	13.2	11.8	11.4	10.4	10.2	10.6	9.4	13.1	9.6	13.1	16.4	14.1	13.7
Na_2O	0.11	0.10	0.10	0.10	0.16	0.10	0.10	0.04	0.04	0.04	0.05	0.08	0.07	0.05	0.10	0.05	0.10	0.04	0.03	0.04	0.04
Cr_2O_3	1.12	0.73	0.91	0.39	0.05	1.17	0.41	0.13	0.15	0.10	0.15	0.05	0.06	0.07	0.03	0.12	0.03	0.12	0.19	0.16	0.15
Total	101.4	101.1	100.0	100.5	100.0	99.7	100.1	100.3	100.3	100.4	100.0	100.1	97.8	99.8	99.5	99.8	100.0	100.0	99.8	99.6	99.9
Ti (ppm)	1,858	1,499	2,038	1,619	2,818	1,685	1,259	839	659	659	839	1,379	1,379	719	1,978	659	1,619	659	480	480	540
Ni	49.5	46.7	68.2	46.9	14.4	49.7	–	92.9	93.4	118.6	93.6	44.5	43.9	75.2	64.7	101.0	44.2	108.9	121.3	87.8	96.3
Sr	0.72	0.65	0.62	0.60	0.78	0.80	0.54	1.81	0.56	1.02	1.45	1.82	3.24	1.46	1.31	0.85	1.32	0.86	0.36	1.03	0.99
Y	23.3	23.9	23.6	23.4	47.8	25.9	0.0	2.9	2.6	1.9	2.9	6.0	5.9	2.4	7.4	2.7	6.4	2.9	2.9	3.1	3.1
Zr	21.6	16.6	15.4	18.5	24.2	25.6	n/a	2.7	3.3	2.2	2.7	4.9	4.3	3.3	15.8	3.3	19.1	3.7	1.9	2.5	2.4
Nb	0.07	0.06	0.07	0.08	0.18	0.09	0.08	0.45	0.38	0.13	0.38	0.24	0.54	0.30	0.21	0.19	0.19	0.19	0.09	0.10	0.00
La	<0.01	0.02	<0.01	<0.01	0.02	0.02	0.02	0.17	0.03	0.03	0.14	0.02	0.20	0.07	0.02	0.03	<0.01	0.03	0.02	0.07	0.08
Ce	0.22	0.18	0.19	0.17	0.15	0.26	0.16	1.32	0.25	0.33	1.19	0.33	1.22	0.73	0.23	0.32	0.26	0.33	0.13	0.45	0.45
Pr	0.10	0.10	0.10	0.09	0.07	0.13	0.08	0.38	0.09	0.14	0.35	0.18	0.40	0.27	0.11	0.13	0.11	0.13	0.04	0.15	0.12
Nd	1.54	1.51	1.38	1.01	0.86	1.95	1.10	3.01	1.01	0.99	2.59	2.22	3.27	2.16	1.23	0.97	1.32	1.13	0.39	1.12	0.99
Sm	1.76	1.55	1.54	1.32	1.25	2.06	1.38	0.68	0.38	0.40	0.68	1.22	1.29	0.67	1.05	0.41	1.06	0.47	0.18	0.36	0.42
Eu	0.77	0.67	0.69	0.56	0.70	0.86	0.58	0.29	0.24	0.24	0.29	0.55	0.59	0.35	0.61	0.27	0.61	0.28	0.12	0.20	0.25
Gd	3.37	2.81	3.07	2.55	4.22	3.85	2.43	0.51	0.51	0.40	0.46	1.10	1.19	0.64	1.71	0.41	1.55	0.54	0.33	0.45	0.43
Tb	0.61	0.55	0.58	0.48	1.00	0.70	0.53	0.08	0.08	0.07	0.08	0.20	0.19	0.08	0.25	0.08	0.21	0.09	0.07	0.07	0.06
Dy	4.06	4.02	4.11	3.86	7.82	4.62	3.86	0.52	0.56	0.40	0.54	1.28	1.35	0.49	1.59	0.51	1.35	0.62	0.56	0.50	0.45
Ho	0.85	0.86	0.87	0.83	1.81	0.96	0.87	0.12	0.10	0.07	0.12	0.25	0.24	0.09	0.30	0.10	0.26	0.11	0.10	0.12	0.13
Er	2.58	2.74	2.60	2.84	5.77	2.85	3.00	0.38	0.32	0.23	0.34	0.66	0.64	0.31	0.82	0.32	0.70	0.33	0.33	0.36	0.38
Tm	0.34	0.37	n/a	0.40	0.81	0.40	n/a	0.05	0.05	0.03	0.05	0.08	0.08	0.04	0.10	0.04	0.08	0.05	0.06	0.06	0.05
Yb	2.42	2.70	2.57	2.94	5.60	2.61	3.34	0.34	0.33	0.21	0.35	0.51	0.55	0.25	0.57	0.28	0.64	0.32	0.32	0.35	0.42
Lu	0.37	0.42	0.40	0.46	0.86	0.40	0.49	0.06	0.08	0.06	0.08	0.08	0.08	0.05	0.10	0.07	0.11	0.05	0.06	0.07	0.05
Hf	0.42	0.27	0.28	0.29	0.32	0.49	0.19	0.05	0.06	0.04	0.05	0.15	0.15	0.07	0.29	0.07	0.32	0.06	0.05	0.05	0.04
Eu/Eu*	0.96	0.98	0.97	0.93	0.93	0.93	0.97	1.50	1.66	1.81	1.58	1.45	1.45	1.63	1.39	2.01	1.44	1.69	1.50	1.51	1.79
$\delta^{18}O$	6.21	6.21	7.04	6.8	8.1	6.67	n/a	5.34	5.34	5.28	5.42	5.37	5.37	5.23	5.54	5.47	n/a	5.42	5.26	5.18	n/a

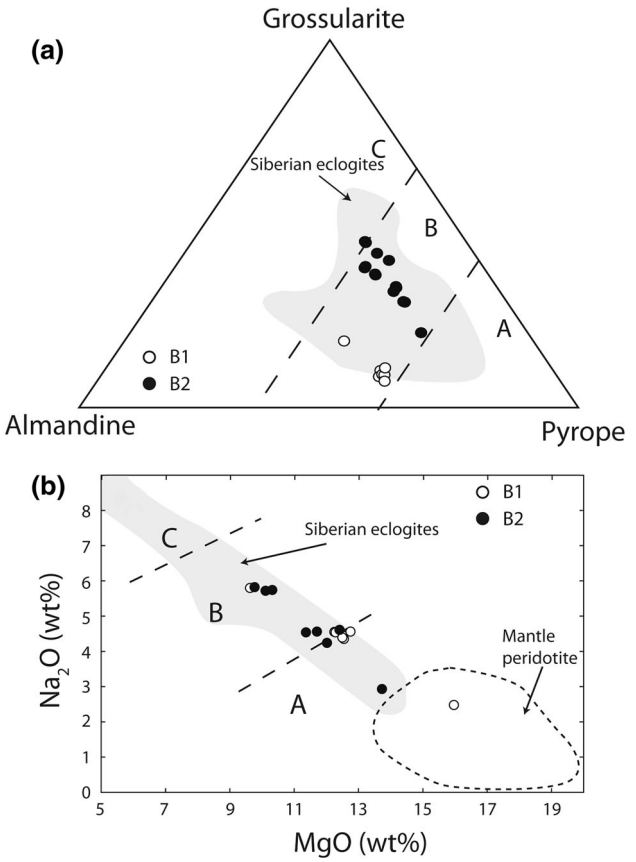

Fig. 2 Major-element compositions of Komsomolskaya garnets and clinopyroxenes. **a** Ca-Fe–Mg garnet ternary plot. **b** Clinopyroxene Na_2O and MgO variations. The A-B-C classification scheme from Taylor and Neal (1989) is shown for comparison. Data for the Siberian eclogite field was compiled from Jerde et al. (1993), Sobolev et al. (1994), Beard et al. (1996), and Snyder et al. (1997). Data for the mantle peridotite field was compiled from Boyd (1989), Johnson et al. (1990), Hauri et al. (1993), Pearson et al. (1994), and Xu et al. (2000)

a maxima at Nd (Fig. 4a). Clinopyroxenes from group B1 are further characterized by small positive Sr anomalies, negative Nb anomalies, and distinct negative Ti anomalies (Fig. 4c). Group B2 clinopyroxenes generally have sub-chondritic HREE, but display enrichments in LREE–MREE (Fig. 4b). Several B2 clinopyroxenes show 'humped' REE patterns, similar to the group B1 clinopyroxenes, whereas some have LREE-enriched patterns (Fig. 4). In contrast to the B1 clinopyroxenes, group B2 clinopyroxenes are characterized by strong positive Sr anomalies, negative Nb anomalies, and small positive Ti anomalies (Fig. 4d).

P–T estimates

Eclogites from this study display no zonation in their mineral chemistry; as such, the major-element compositions can be used to estimate the final equilibration temperatures of these samples. We adopt the thermometers of Krogh (1998) and Ellis and Green (1979), which are based on Mg–Fe^{2+} exchange between clinopyroxene and garnet. No barometer is currently available for the clinopyroxene–garnet assemblage. Consequently, a number of temperatures have been calculated for a range of hypothetical pressures for each sample. The resulting P–T lines from these calculations were then projected onto the Udachnaya geotherm (Howarth et al. 2014) for each sample, in order to estimate the equilibration pressures and temperatures (Fig. 7). This method assumes that both peridotites and eclogites were equilibrated to the same geotherm within the lower lithosphere. No geotherm has been defined for the lithosphere beneath Komsomolskaya; therefore, the well-constrained geotherm from the neighboring Udachnaya pipe was used in order to make these estimates (Boyd 1984; Howarth et al. 2014). This geotherm was quantitatively fitted based on P–T estimates from a large suite of peridotites using the FITPOLT program (Mather et al. 2011; Howarth et al. 2014). The uncertainty on the equilibrium temperatures using this method has been estimated to be ±50 °C, which corresponds to a relative depth-estimate uncertainty of ±10 km. The equilibrium temperatures and depths for the Komsomolskaya eclogite suite are given in Table 2. Both group B1 and B2 overlap in their P–T estimates. Group B1 spans a range of temperatures and pressures of 985–1,190 °C and 44–55 kbar, whereas group B2 samples have a range of 1,003–1,110 °C and 43–56 kbar, corresponding to depths between 153 and 199 km for B1 samples and 159–180 km for B2 samples, consistent with the diamondiferous nature of these eclogites (Fig. 7).

Discussion

Prior to interpreting the origins of this eclogite suite, it is important to consider the potential effects of any secondary modification of eclogite chemistry. In particular, metasomatism is a ubiquitous process within the SCLM, which can significantly alter the chemistry and mineral proportions of mantle xenoliths (e.g., Dawson 1984; Menzies et al. 1987; Boyd et al. 1997; Misra et al. 2004; Jacob et al. 2009). By considering reconstructed bulk-rock chemistry, which is able to exclude the effects of fine grain (<10 μm) interstitial metasomatism, the primary eclogite chemical characteristics can be identified and subsequently used for interpretations.

Effects of metasomatism

Metasomatism is generally described as being either 'modal' (Dawson and Smith 1977) or 'cryptic' (Dawson

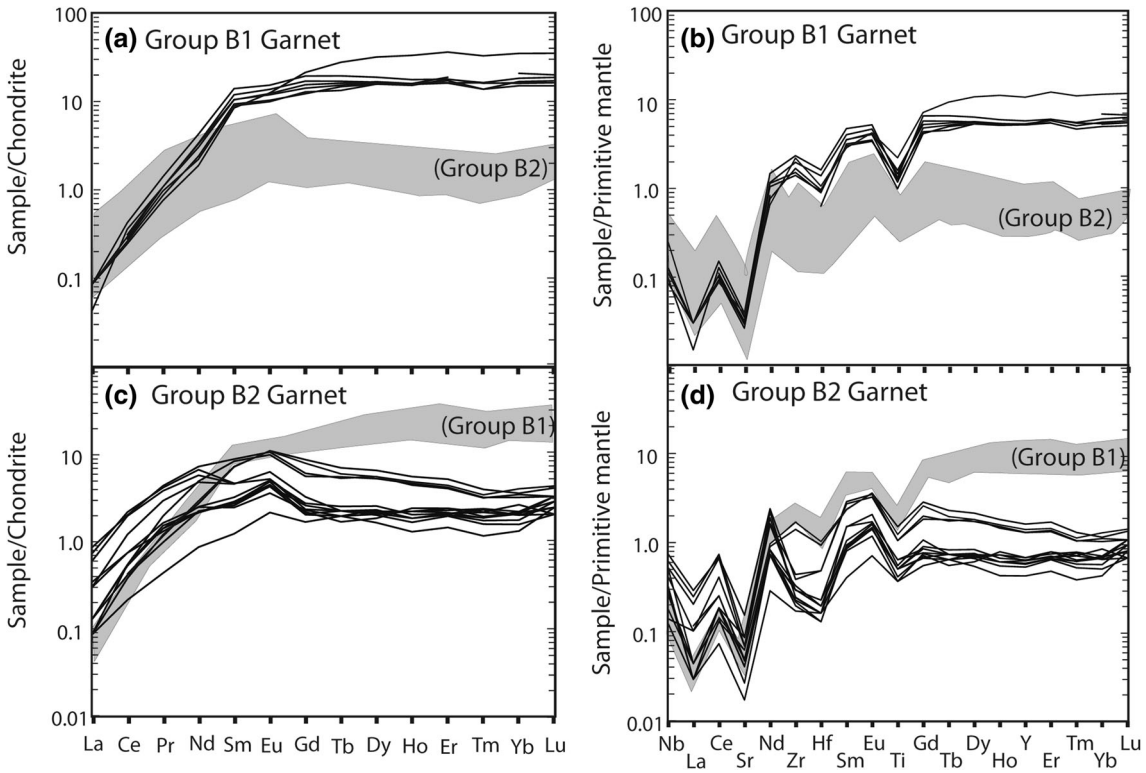

Fig. 3 **a**, **b** Chondrite-normalized REE abundances of group B1 and B2 Komsomolskaya garnets. *Gray fields* show the range of values from opposing group. **c**, **d** Primitive mantle-normalized, trace-element abundances of group B1 and B2 Komsomolskaya garnets. *Gray fields* show the range of values from opposing group. Elements were arranged in the order of decreasing compatibility. All normalization factors from McDonough and Sun (1995)

1984). The former is used to describe changes in the modal proportions due to the addition of metasomatic phases (e.g., MARID—*M*ica-*A*mphibole-*R*utile-*I*lmenite-*D*iopside—rocks; phlogopite-bearing garnet peridotites). In contrast, the latter is identified by LREE–MREE enrichments in the primary minerals, without the occurrence of metasomatic phases. In this suite of eclogites, we find little evidence for significant modal metasomatism, with no phlogopite identified. Further, the presence of phlogopite co-existing in equilibrium with garnet can be inferred by lower Hf and Y, for a given Zr concentration, due to the partitioning of these elements between the garnet and phlogopite. Komsomolskaya samples consistently fall on the phlogopite-free trends (Fig. 8; Griffin et al. 1999; Jacob et al. 2009). Fine-grained interstitial metasomatic mineral assemblages have also been identified in these samples. Such assemblages are typically the result of late-stage percolating fluids (e.g., Misra et al. 2004); however, they occur in small quantities and do not appear to significantly affect the modal proportions of the eclogite.

All clinopyroxene and group B2 garnets display LREE and MREE enrichments relative to the HREE, consistent with minor amounts of cryptic metasomatism. The lack of chemical zoning preserved in minerals from these samples suggests that the cryptic metasomatism must have occurred over relatively large timescales, predating entrainment into the host kimberlite. Diffusion calculations on garnet Ca content from peridotites have suggested that zoning can be overprinted in times on the order of 1–2 Ma (Howarth et al. 2014). Using mineral/melt partition coefficients (Barth et al. 2002a), the melts in equilibrium with clinopyroxene compositions are LREE-enriched (Fig. 9). Similar LREE-enriched fluids have been reported from peridotite mineral/melt reconstructions and are interpreted to represent metasomatism by circulating kimberlitic fluids, just prior to eruption (Ionov et al. 2010; Doucet et al. 2013; Howarth et al. 2014). Notably, due to the relatively low HREE concentrations in the group B2 garnets, the LREE–MREE enrichments in these samples have imparted sinusoidal-like patterns, similar to those observed in some reported metasomatized harzburgitic garnets (e.g., Ionov et al. 2010).

In summary, we conclude that modal metasomatism has not significantly altered the mineralogy of the Komsomolskaya suite, in contrast, perhaps, to other mantle eclogites worldwide (e.g., Roberts Victor; Greau et al. 2011). However, LREE–MREE concentrations in mineral separates have clearly been affected by cryptic metasomatism, and thus should be treated with caution in subsequent

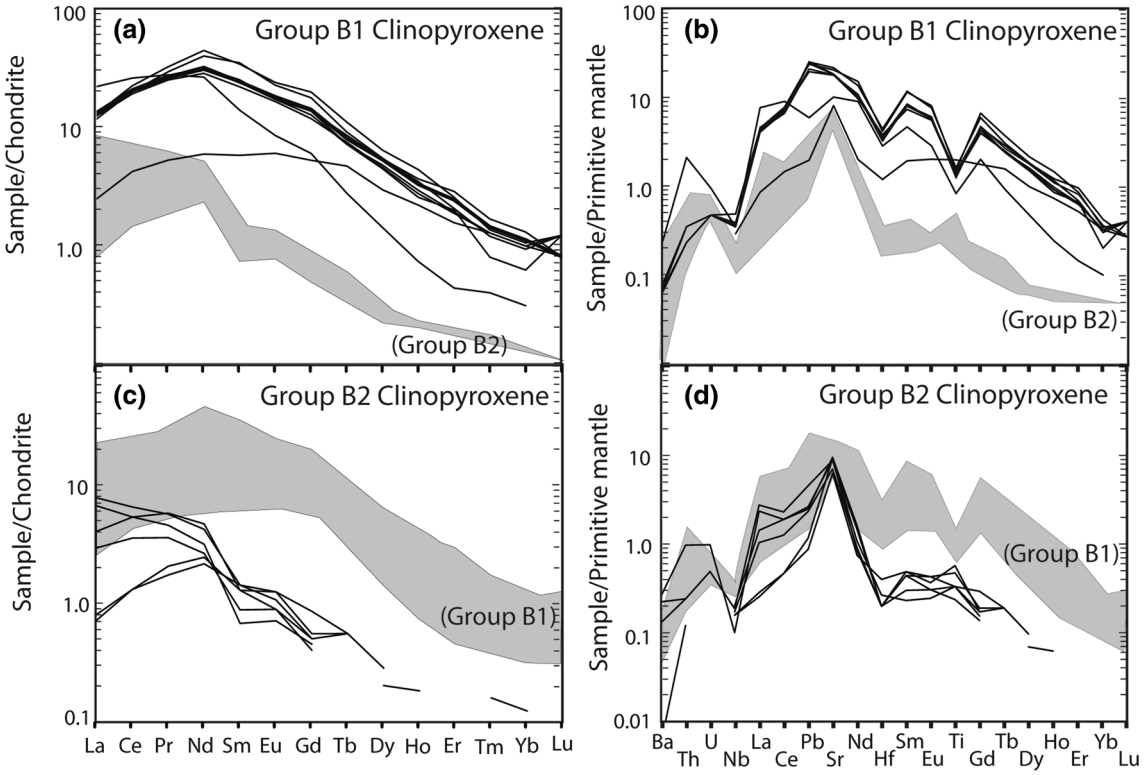

Fig. 4 **a**, **b** Chondrite-normalized REE abundances of group B1 and B2 Komsomolskaya clinopyroxenes. *Gray fields* show the range of values from opposing group. **c**, **d** Primitive mantle-normalized, trace-element abundances of group B1 and B2 Komsomolskaya clinopyroxenes. *Gray fields* show the range of values from opposing group. Elements were arranged in the order of decreasing compatibility. All normalization factors from McDonough and Sun (1995)

interpretations. Importantly, the most-compatible elements (i.e., HREE, HFSE) are the least affected during cryptic metasomatism (e.g., Schmickler et al. 2004), and therefore, they are the focus in subsequent sections, in particular, for interpretations based on bulk-rock reconstructions. While evidence suggests that metasomatism affects mineral chemistry, only thoroughly pervasive metasomatism would be expected to significantly modify oxygen isotopes; as such, we consider the oxygen isotope systematics reported here to reflect primary values.

Bulk-rock reconstruction systematics

The occurrence of fine-grained interstitial, metasomatic mineral assemblages in the diamondiferous Komsomolskaya suite can severely affect measured bulk-rock systematics. By reconstructing bulk-rock values using primary mineral compositions and modal estimates, the effects of this metasomatism can be excluded, making it possible to identify primary chemical signatures. However, for small sample sizes, modal estimates can have uncertainties of up to 50 % (Jacob et al. 2009). Consequently, this can lead to uncertainties in calculated major-element concentrations of up to several weight-percent. However, trace-element patterns of bi-mineralic eclogites are relatively impervious to large changes in garnet and clinopyroxene model abundance, and as such, are valid to use (e.g., Jerde et al. 1993). Reconstructions reported here are based on visually estimated modes of 39–60 % garnet, 60–39 % clinopyroxene, and <1 % rutile (Table 3).

The LREEs and MREEs are the most susceptible to modification during metasomatism. In light of the cryptic metasomatism highlighted above, the concentrations of these elements must be treated with caution, as they may not represent primary compositions. Reconstructed major-element compositions exhibit MgO contents between 10 and 16 wt%. Group B1 eclogites have Mg# $\leq$ 70, exhibiting elevated MgO (average $\sim$13 wt%) and Cr_2O_3 ($\sim$1 wt%). Group B2 eclogites have Mg# > 70, FeO < 7 wt%, and Al_2O_3 ranging from of 13–15 wt%.

Reconstructed REE profiles are relatively flat (Fig. 10); group B1 profiles have supra-chondritic values, whereas those of group B2 have sub-chondritic to slightly supra-chondritic REE contents. The MREEs for all samples are slightly enriched, resulting in a 'humped' profile peaking at Nd. This is most likely a residual artifact of the cryptic metasomatism, previously identified. Samples from group B1 do not exhibit Eu anomalies, but do display moderately

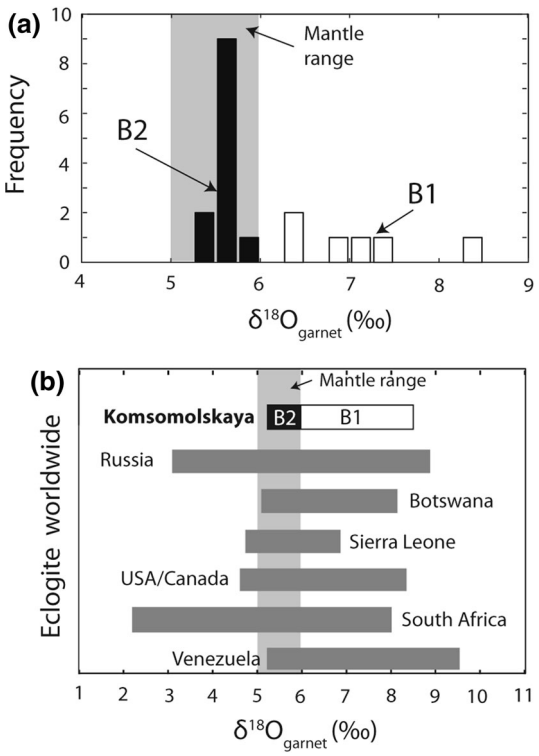

Fig. 5 **a** Histogram of garnet oxygen isotope compositions. Field of mean mantle values after Mattey et al. (1994), Valley et al. (1998), and Valley (2003). **b** Oxygen isotope data from this study with respect to eclogites worldwide (after Schulze 2003 and Jacob 2004)

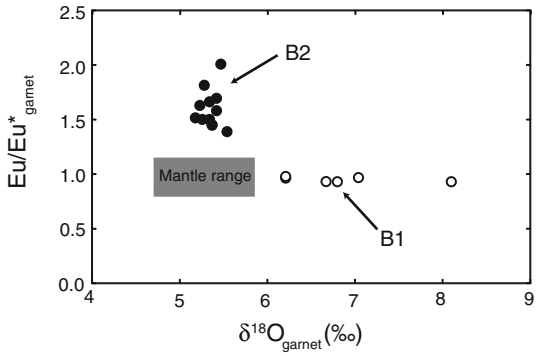

Fig. 6 Oxygen isotopes versus Eu anomaly (Eu/Eu^*_{garnet}). Field of mean mantle $\delta^{18}O$ values after Mattey et al. (1994), Valley et al. (1998), and Valley (2003)

positive Sr anomalies. In contrast, group B2 bulk-rock compositions exhibit both Eu and Sr anomalies. Both B1 and B2 groups display flat-reconstructed HREE patterns; these profiles bear a striking resemblance to typical oceanic protoliths (Fig. 10). Group B1 eclogites are similar to typical basaltic compositions, whereas group B2 eclogites resemble anorthositic-gabbro compositions, potentially reflecting their low-pressure crustal protoliths.

Implications for eclogite origin: oceanic crust versus mantle cumulates

There are several diagnostic indicators that have classically been used to advocate a low-pressure origin for the protoliths of the eclogites, such as elevated $\delta^{18}O$ values, distinct S isotopes, bulk-rock REE systematics, and Eu anomalies (e.g., Jagoutz et al. 1984; Jacob and Foley 1999; Taylor et al. 2000 Farquhar et al. 2002; Spetsius and Taylor 2008). Recently, however, a number of these lines of evidence have been suggested to represent metasomatism of high-pressure mantle cumulates that form at the base of the lithosphere (Griffin and O'Reilly 2007; Greau et al. 2011). These lines of evidence are considered in the following section in order to place constraints on the origin of the Komsomolskaya eclogites.

Evidence from Rare Earth Elements and Mineral Chemistry

The presence of positive Sr and Eu anomalies in eclogite bulk-rock compositions, (Fig. 10), is typically interpreted to reflect an origin as a mid/lower plagioclase-rich crustal cumulate (e.g., Barth et al. 2002b; Schmickler et al. 2004; Jacob and Foley 1999). However, several authors have suggested that positive Sr and Eu anomalies can also be introduced to bulk-rock compositions through metasomatism and, consequently, do not preserve primary signatures (Greau et al. 2011; Huang et al. 2012). Bulk-rock trace-element reconstructions exclude such contamination; however, group B2 eclogites still exhibit positive Sr and Eu anomalies. These features can only reflect the accumulation of plagioclase and are not expected from an origin as high-pressure cumulates, as plagioclase is not stable at the estimated pressures for these samples (Borghini et al. 2010). High-pressure experimental results have shown that garnet and clinopyroxene occur together at the liquidus at pressures >17 kbar (e.g., Jacob 2004). At such depths, mantle-cumulates are expected to fractionate the HREEs due to the accumulation of garnet (Smart et al. 2012). However, this is not the case; both B1 and B2 eclogites have flat-HREE patterns, consistent with shallower origins. Further, Jacob (2004) has argued that it is unlikely that such cumulates would form in the first place. They suggest that olivine (a rare mineral in eclogites) should be the first phase to accumulate at geologically realistic conditions for primary mantle melts.

In general, group B2 reconstructed REE patterns closely resemble typical oceanic gabbros (e.g., Bach et al. 2001), with CaO and Al_2O_3 suggesting plagioclase-rich cumulates. In contrast, group B1 eclogites exhibit only positive Sr anomalies and have higher REE concentrations. This is expected for the basaltic portions of oceanic crust, where

Table 2 Major-, and trace-element data of Komsomolskaya clinopyroxenes

Group	K1a 1	K1b 1	K9 1	K10 1	K14a 1	K15a 1	K16 1	K4 2	K5a 2	K5b 2	K11 2	K12 2	K13 2
SiO_2 (wt%)	55.2	55.1	55.1	55.8	55.5	54.8	55.3	55.2	55.5	55.5	55.4	55.2	55.6
TiO_2	0.35	0.18	0.30	0.31	0.43	0.27	0.33	0.07	0.12	0.10	0.05	0.07	0.07
Al_2O_3	6.6	2.1	6.3	6.7	9.4	6.2	6.5	7.9	10.5	10.2	8.9	5.8	9.4
Cr_2O_3	0.96	2.81	0.82	0.44	0.05	1.16	0.62	0.10	0.05	0.04	0.10	0.15	0.15
MgO	12.3	16.0	12.4	12.4	9.6	12.3	12.8	12.0	10.1	10.3	11.7	13.7	11.4
CaO	13.7	18.9	13.8	13.5	13.1	14.1	13.1	17.5	15.0	15.2	16.8	19.1	16.5
MnO	0.06	0.08	0.06	0.07	0.05	0.07	0.08	<0.05	<0.05	<0.05	<0.05	<0.05	<0.05
FeO	5.5	2.1	5.7	6.1	5.5	5.4	6.3	2.5	2.7	2.6	1.9	2.3	1.8
Na_2O	4.55	2.48	4.61	4.56	5.8	4.54	4.56	4.24	5.72	5.74	4.56	2.93	4.54
K_2O	0.23	0.05	0.21	0.22	0.15	0.22	0.21	0.13	0.08	0.09	0.16	0.26	0.22
Total	99.43	99.79	99.43	100.05	99.64	99.02	99.65	99.66	99.67	99.86	99.55	99.52	99.55
Ti (ppm)	2,098	1,079	1,798	1,858	2,578	1,619	1,978	420	719	599	300	420	420
Sr	454.1	212.7	375.4	375.3	170.8	375.8	429.7	192.7	127.1	185.6	142.3	177.5	179.6
Zr	12.0	24.4	23.8	24.4	15.2	20.6	22.5	1.1	1.7	1.3	1.0	1.1	1.2
Nb	0.25	0.25	0.32	0.25	0.21	0.27	0.35	0.14	0.11	0.11	0.12	0.13	0.07
La	2.80	5.26	3.19	3.11	0.59	3.16	3.11	0.95	0.17	0.19	0.69	1.82	1.56
Ce	12.33	16.04	12.65	12.99	2.60	12.74	13.81	3.24	0.80	0.80	2.16	3.94	3.25
Pr	2.74	2.58	2.48	2.56	0.49	2.48	3.02	0.53	0.16	0.19	0.33	0.52	0.42
Nd	18.35	12.16	14.63	14.51	2.72	14.67	20.40	2.12	0.98	1.11	1.20	1.91	1.42
Sm	5.20	2.07	3.58	3.74	0.86	3.60	5.08	0.19	0.21	0.19	0.13	0.21	0.10
Eu	1.28	0.48	0.95	0.97	0.34	1.02	1.35	0.05	0.06	0.07	0.05	0.07	0.04
Gd	3.54	1.20	2.68	2.73	1.05	2.82	3.96	0.10	0.10	0.11	0.08	0.17	0.09
Tb	0.33	0.10	0.28	0.31	0.17	0.29	0.40	–	0.02	0.02	–	0.02	–
Dy	1.35	0.35	1.30	1.33	0.73	1.31	1.58	0.05	–	–	–	0.07	0.06
Ho	0.19	0.04	0.18	0.20	0.12	0.18	0.24	0.01	–	–	–	–	–
Er	0.33	0.07	0.37	0.46	0.25	0.39	0.41	–	–	–	–	–	–
Yb	0.15	0.05	0.15	0.21	0.16	0.18	0.17	–	–	–	–	0.02	–
Lu	0.03	<0.01	<0.01	0.02	0.02	0.02	0.03	–	–	–	–	–	–
Hf	1.37	0.88	1.13	1.12	0.37	1.05	1.29	0.06	0.12	0.06	0.06	0.06	0.08
Pb	1.77	0.42	1.48	1.38	0.14	1.48	1.67	0.17	0.06	0.08	0.16	0.31	0.18
T (°C)	1,011	1,003	1,070	1,080	1,195	1,070	1,090	1,120	1,190	1,190	1,075	985	1,055
P (Kbar)	44	49	47	48	55	48	51	51	56	55	49	43	47
Depth (km)	160	156	168	170	195	170	175	181	199	195	174	153	167

The equilibration temperature and depth estimates for each xenolith are also listed

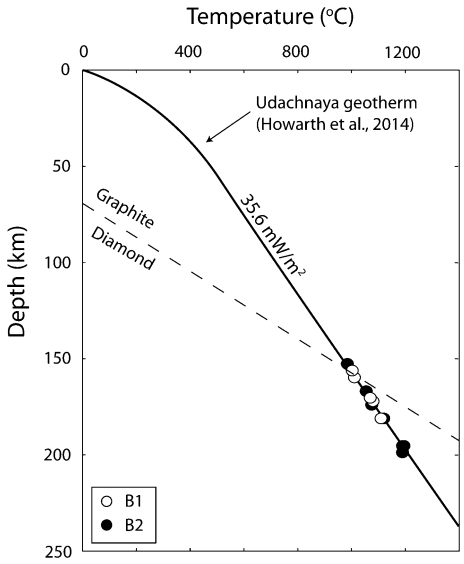

Fig. 7 P-T estimates calculated using the method of Krogh (1998) and Ellis and Green (1979). Depths were estimated using the Udachnaya geotherm from Boyd (1984) and Howarth et al. (2014). Graphite–diamond stability line is after Kennedy and Kennedy (1976)

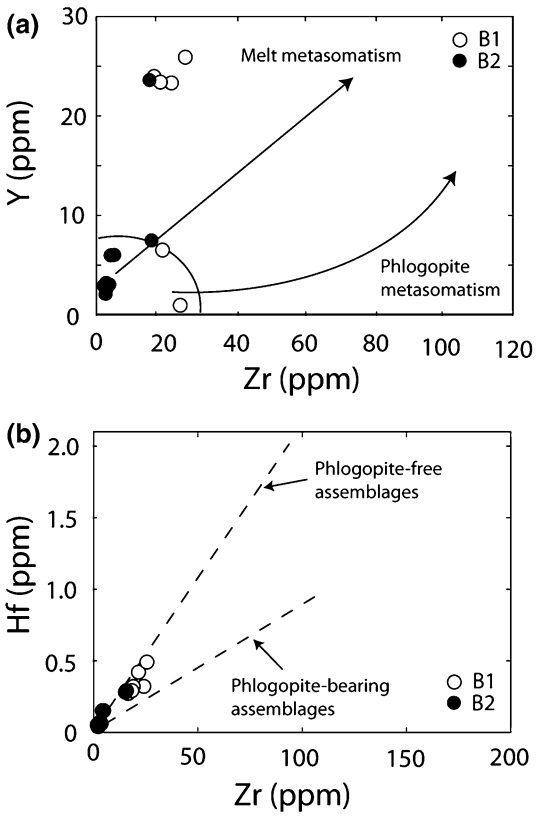

Fig. 8 **a** Garnet Y versus Zr and **b** Garnet Hf versus Zr. The trends illustrate garnet compositions in equilibrium with-phlogopite and without-phlogopite (after Griffin et al. 1999 and Jacob et al. 2009)

clinopyroxene is more abundant in the protolith. Eu is more compatible in plagioclase over clinopyroxene; therefore, large Eu anomalies are only expected in plagioclase-rich

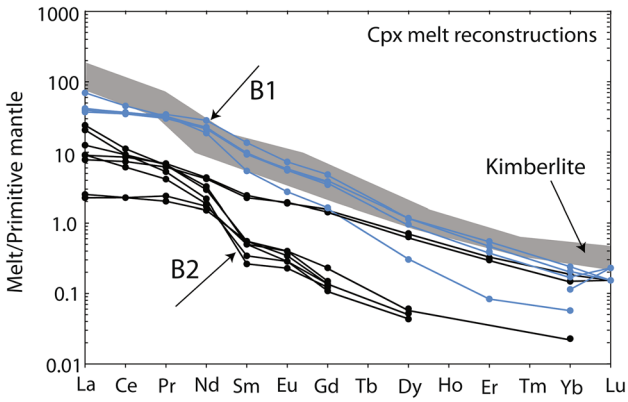

Fig. 9 Primitive mantle-normalized (McDonough and Sun 1995) REE patterns for hypothetical melts in equilibrium with clinopyroxene, calculated using mineral/melt partition coefficients from Barth et al. (2002a). *Gray field* shows the range of Udachnaya kimberlite compositions from Kamenetsky et al. (2012)

rocks (Fig. 10). The relative proportions of plagioclase and clinopyroxene within the potential protoliths of these eclogites are reflected by Sr/Lu, which is high in plagioclase-rich rocks (Schmickler et al. 2004). Group B1 samples have Sr/Lu ranging from 193–778, whereas group B2 samples have Sr/Lu ranging from 1,082 to 1,978. These ratios are consistent with a basaltic upper-oceanic crustal protolith for B1 eclogites, whereas group B2 eclogites are interpreted to represent a mid-lower-crustal cumulate protolith.

Additionally, clinopyroxenes from eclogites worldwide are distinct from high-pressure liquidus pyroxenes produced in experiments (Eggins 1992) and from garnet clinopyroxenite layers found within massif peridotites (Pearson and Nixon 1995). This distinction is reflected by Jd % and Ca-Tschermak's % (CaTs %) variations (Fig. 11). Additionally, P–T estimates from this suite suggest that these eclogites were re-equilibrated at a range of mid-lithospheric depths. This is inconsistent with the mantle-cumulate hypothesis, which suggests that such high-pressure cumulates form at the base of the lithosphere (Greau et al. 2011).

Evidence from oxygen isotope ratios

High $\delta^{18}O$ values were one of the first lines of evidence proposed for the low-pressure origin of eclogite protoliths, due to the small fractionation of oxygen isotopes at high temperatures or during subduction (e.g., MacGregor and Manton 1986; Jagoutz et al. 1984). This interpretation has recently been challenged by Griffin and O'Reilly (2007), who argued that elevated oxygen isotope values in eclogites are the result of metasomatic processes within the SCLM. However, if high-$\delta^{18}O$ metasomatic fluids were

Table 3 Reconstructed major- and trace-element data of Komsomolskaya eclogites, assuming a cpx:gt:rut proportion of 60:39:1

Reconstructed Bulk-rock: cpx60: gt39:rutile1	K1a B1	K1b B1	K9 B1	K10 B1	K14a B1	K15a B1	K16 B1	K4 B2	K5a B2	K5b B2	K11 B2	K12 B2	K13 B2
SiO_2 (wt%)	49.5	49.4	49.4	49.8	49.2	49.1	49.5	49.3	49.5	49.2	49.7	49.6	49.7
TiO_2	0.3	0.2	0.3	0.3	0.4	0.3	0.3	0.1	0.2	0.2	0.1	0.1	0.1
Al_2O_3	12.8	10.1	12.6	12.9	14.5	12.4	12.7	13.8	15.3	14.9	14.5	12.7	14.8
Cr_2O_3	1.0	2.0	0.9	0.4	0.1	1.2	0.6	0.1	0.1	0.0	0.1	0.2	0.2
MgO	13.6	15.8	13.7	13.8	10.5	13.5	13.9	11.8	10.2	10.3	12.3	14.8	12.5
CaO	9.7	12.6	9.7	9.4	10.5	10.0	9.6	16.0	14.7	14.8	15.0	14.6	14.2
MnO	0.2	0.2	0.2	0.2	0.2	0.2	0.2	0.1	0.1	0.1	0.1	0.1	0.1
FeO	10.3	8.4	10.3	10.5	10.7	9.8	10.4	6.0	6.3	6.1	5.2	5.7	5.1
Na_2O	2.8	1.5	2.8	2.8	3.5	2.8	2.7	2.6	3.5	3.5	2.8	1.8	2.7
Sr ppm	182	85	151	150	69	151	155	78	52	76	57	71	72
Zr	17.8	19.7	18.7	20.8	20.6	23.6	–	2.1	3.7	3.1	2.6	1.6	2.0
Nb	0.14	0.14	0.17	0.15	0.19	0.16	0.15	0.28	0.19	0.37	0.16	0.11	0.09
La	1.13	2.12	1.28	1.24	0.25	1.28	1.21	0.46	0.08	0.20	0.29	0.74	0.67
Ce	5.06	6.52	5.17	5.30	1.62	5.25	5.00	2.01	0.52	1.05	1.06	1.65	1.57
Pr	1.16	1.09	1.05	1.08	0.32	1.07	1.01	0.42	0.17	0.32	0.21	0.23	0.26
Nd	8.26	5.77	6.68	6.41	1.98	7.04	6.23	2.40	1.72	2.41	1.16	1.00	1.24
Sm	3.14	1.76	2.36	2.29	1.02	2.68	2.25	0.48	0.82	0.85	0.33	0.19	0.26
Eu	0.97	0.59	0.80	0.72	0.48	0.92	0.74	0.19	0.35	0.38	0.19	0.10	0.14
Gd	3.44	2.17	2.91	2.62	2.32	3.44	2.47	0.32	0.70	0.76	0.36	0.27	0.31
Tb	0.50	0.37	0.46	0.41	0.50	0.54	0.42	0.05	0.07	0.12	0.05	0.05	0.04
Dy	2.98	2.55	2.99	2.85	3.57	3.30	2.76	0.34	0.77	0.81	0.37	0.36	0.32
Ho	0.59	0.53	0.59	0.58	0.80	0.65	0.58	0.08	0.15	0.14	0.07	0.06	0.07
Er	1.68	1.67	1.71	1.89	2.46	1.87	1.92	0.20	0.40	0.38	0.20	0.20	0.22
Yb	1.51	1.64	1.60	1.85	2.34	1.64	2.04	0.21	0.31	0.33	0.19	0.20	0.21
Lu	0.23	0.25	0.24	0.28	0.36	0.25	0.31	0.05	0.05	0.05	0.03	0.04	0.04
Hf	0.60	0.71	0.62	0.62	0.42	0.71	0.53	0.05	0.14	0.11	0.06	0.05	0.06
Mg #	70.2	77.0	70.2	69.9	63.8	71.1	70.5	77.8	74.3	75.1	80.8	82.3	81.2
Sr/Lu	778	339	627	530	193	608	506	1,624	1,082	1,587	1,914	1,978	1,725

generated within the mantle, it is generally agreed they would exchange readily with surrounding peridotite (Pearson et al. 2003). Such rapid buffering in $\delta^{18}O$ is reflected in part by the uniformly homogenous nature of $\delta^{18}O$ values in mantle peridotites worldwide, despite often displaying extensive trace-element metasomatism (Mattey et al. 1994; Chazot et al. 1997; Eiler 2001; Valley 2003). In addition, extremely large fluid/rock ratios are needed in order to significantly change the oxygen isotope ratios; this would result in crystallization of hydrous phases, which are not present in this sample suite. Further, studies have shown that the oxygen-isotopic compositions of metasomatic mineral assemblages (i.e., MARID minerals) have a limited range, generally overlapping mantle values (Rehfeld et al. 2008; Jacob et al. 2009). Therefore, significant deviations from the average mantle value in eclogites, such as reported for the B1 samples, are generally considered to reflect their original, pre-subduction signature—not metasomatism.

The elevated $\delta^{18}O$ values for the B1 eclogites overlap with the range of $\delta^{18}O$ values reported for the uppermost crustal units in ophiolites and drill-cores of fresh oceanic basalts (e.g., Gregory and Taylor 1981; Alt and Bach 2006). The higher $\delta^{18}O$ values in oceanic basalts reflect low-temperature (<350 °C) interaction with seawater in the upper basaltic portions of the oceanic crust (Muehlenbachs and Clayton 1972; MacGregor and Manton 1986; Jacob and Foley 1999; Carmody et al. 2013). When considered in combination, the REE profiles that extend up to 10 × chondritic values, the lack of Eu anomalies, and elevated, above-mantle $\delta^{18}O$ values are all consistent with an upper-crust basaltic protolith for B1 eclogites (Fig. 6).

The B2 eclogites display $\delta^{18}O$ values within the range of pristine mantle values. There are three possible

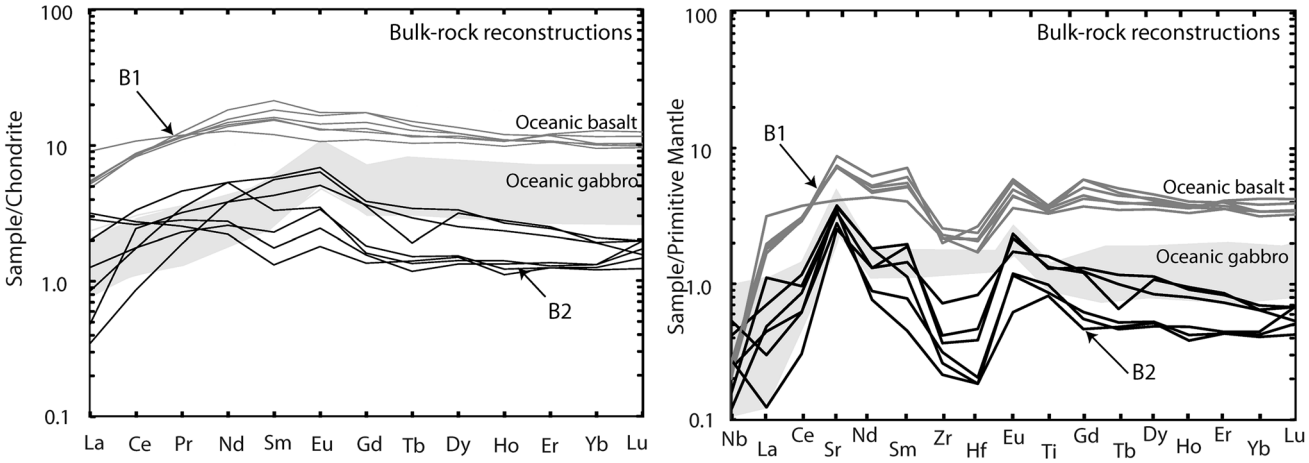

Fig. 10 Chondrite and Primitive mantle-normalized bulk-rock reconstructions for group B1 and B2 eclogites. The data for oceanic basalt and gabbro fields were compiled from the PetDB database (http://www.petdb.org)

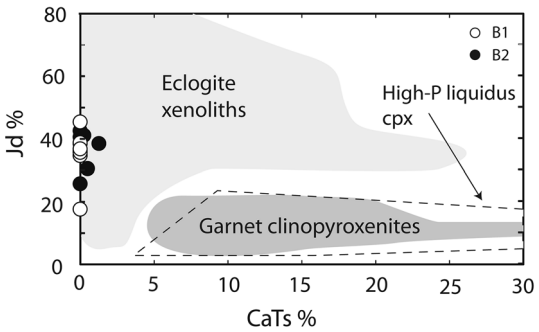

Fig. 11 Clinopyroxene Jadeite % versus CaTs % for Komsomolskaya eclogites. The data for the worldwide eclogite field were compiled from Irving (1974), Garnet Clinopyroxenite from Pearson and Nixon (1995), and data for high-pressure liquidus clinopyroxenes from Eggins (1992)

interpretations for these data: (1) These samples represent cumulates from high-pressure melts within the mantle, and as such, are expected to have mantle $\delta^{18}O$ values; (2) These samples were situated deep in an oceanic crustal pile, where there has been either insignificant hydrothermal alteration or where hydrothermal fluids at low water/rock ratio have reached equilibrium with the surrounding rock (Hart et al. 1999); and (3) These samples have undergone metasomatism by fluids with mantle-like $\delta^{18}O$ values, re-equilibrating their $\delta^{18}O$ values. It is difficult to rule out metasomatism for the origin of the B2 $\delta^{18}O$ values. Some gabbroic portions of crust are reported to have lower than mantle $\delta^{18}O$ values, due to the effects of high-temperature (>350 °C) hydrothermal interaction (e.g., Gregory and Taylor 1981). Therefore, metasomatism within the mantle by fluids with mantle-like oxygen isotopes would increase the $\delta^{18}O$ values of the B2 eclogites. This interpretation is consistent with the LREE–MREE-enriched cryptic metasomatism observed. However, irrespective of the extent of metasomatism the B2 eclogites underwent, the presence of Eu anomalies and flat-HREE patterns in bulk-rock reconstructions cannot be generated from high-pressure mantle cumulates or by metasomatic modifications, and thus is a primary signature. It is only when considering both oxygen isotope values *and* major- and trace-element systematics that an oceanic crustal protolith can be inferred for the B2 eclogites.

Effects of partial melting

It is evident from the previous section that the reconstructed trace-element compositions for the B1 eclogites have basaltic affinities (i.e., higher REE concentrations, low Sr/Lu). However, reconstructed major-element compositions display elevated MgO (>13 wt%) and Cr_2O_3 (~1 wt%), in addition to low SiO_2 (~49 wt%), relative to typical basalts. This has previously been interpreted in other eclogite suites as evidence of a picritic protolith, consistent with the proposed picritic/komatiitic nature of Archean parental magmas (e.g., Arndt 1983; Nisbet and Fowler 1983; Ireland et al. 1994; Jacob and Foley 1999). However, before such conclusions can be reached, the effects of partial melting during subduction must be considered, as these processes can significantly alter major-element chemistry. For instance, moderate degrees of partial melting of eclogites are thought to be the source for TTG complexes found within the basement of cratonic areas (Ireland et al. 1994; Rudnick 1995; Ziaja et al. 2013). On the order of 20–30 %, partial melting has been suggested to be a reasonable estimate to generate TTG melts worldwide (Rudnick 1995; Jacob and Foley 1999; Tappe et al. 2011). However, the extent to which partial melting

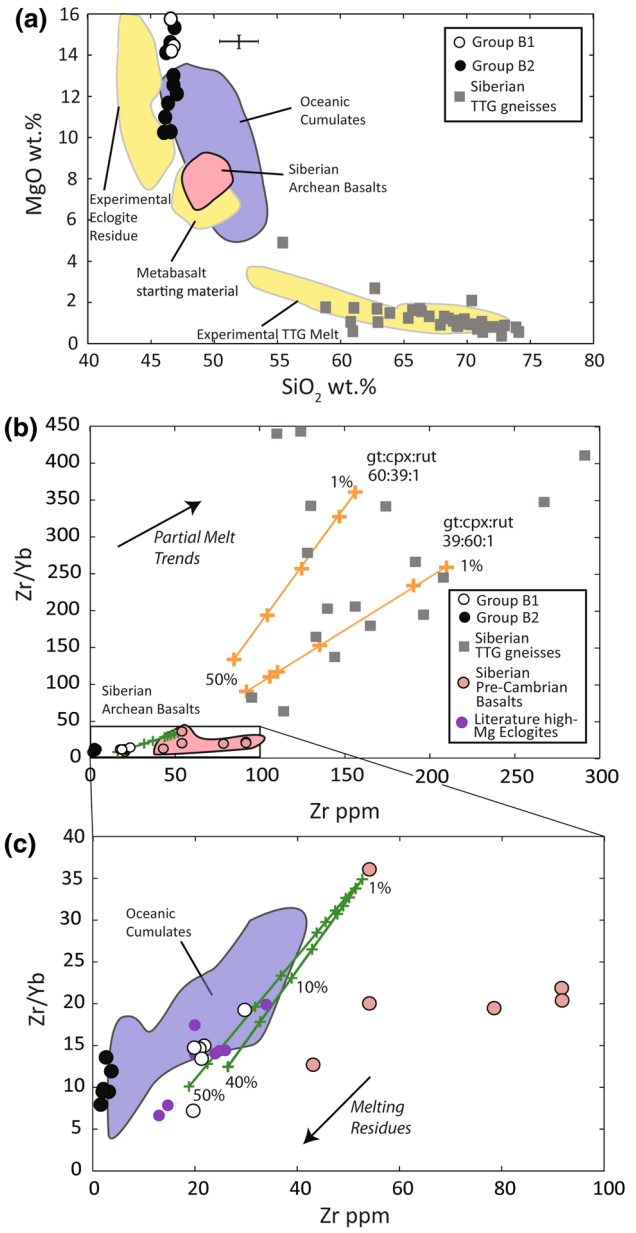

◀**Fig. 12** **a** Reconstructed MgO versus SiO_2 of Komsomolskaya eclogites and late-Archean Siberian TTG melts adapted from Tappe et al. 2011 [TTG data from Donskaya et al. 2009; Turkina et al. 2009, and present day oceanic cumulates compiled from the PetDB database (http://www.petdb.org)]. *Error bar* encompasses the differences in concentrations by varying the modal range between 39:60:1 to 60:39:1, garnet:clinopyroxene:rutile. *Yellow fields* are for experimentally produced TTG melts, corresponding residues, and starting metabasalts from Rapp and Watson (1995). **b** Zr/Yb versus Zr ppm of Komsomolskaya eclogites and late-Archean Siberian TTG melts. Batch melting modeling of typical Siberian Archean basalts (*Orange lines*) is able to explain the wide range of Siberian TTG melts by 5–40 % partial melting, and by varying the proportion of garent:cpx:rut in the source from 60:39:1 to 39:60:1. **c** Zr/Yb versus Zr ppm of Komsomolskaya eclogites, Siberian Precambrian basalts (Jahn et al. 1998) and present day Oceanic Cumulates (compiled from the PetDB database). Calculated melt residues (*Green lines*) encompass the range of Zr/Yb values reported for the B1 eclogites. The B2 eclogites, however, overlap the range of Zr/Yb reported for typical oceanic cumulates, indicating that the group B2 eclogites may not have experience significant melt extraction. Other occurrences of high-Mg eclogites have been plotted for comparison (data from Jacob and Foley 1999; Barth et al. 2002b)

affects the eclogite major-element chemistry is difficult to quantify. Experimental studies have shown that melting of basaltic rocks will yield SiO_2-rich and MgO-poor melts (Fig. 12), leaving a refractory SiO_2-poor and MgO-rich residue (Rudnick 1995; Rapp and Watson 1995; Pertermann and Hirschmann 2003; Ziaja et al. 2013). Indeed, the major-element systematics of group B1 eclogites is consistent with melt extraction from basaltic compositions (Fig. 12a). Trace-element chemistry also reflects a melt-extraction event. Using mineral modes between 39:60 to 60:39 garnet:clinopyroxene, with trace (<1 %) rutile, and with the use of experimentally derived partition coefficients for eclogites at pressures of 3 Ga (Barth et al. 2002a), we calculate that between 5–40 % batch partial melting of a metamorphosed basalt is required to account for the full range of TTG compositions reported from the Siberian craton (Orange lines, Fig. 12b). Calculated residues from such melting are plotted in green (Fig. 12b, c) and encompass the range of Zr/Yb measured in the group B1 eclogites and other high-MgO eclogites globally. This clearly highlights the intimate link between lithosphere and craton formation via subduction.

It is important to note that group B2 'oceanic-cumulate' eclogites also extend to high-MgO and low-SiO_2 contents, as well as displaying low Zr/Yb within the range of the 'basaltic' group B1 eclogites. However, it is not immediately apparent whether these samples underwent significant partial melting. It is unlikely that such refractory protoliths, for example, plagioclase-rich cumulates, would have undergone significant partial melting during subduction. This is reflected by the fact that these samples fall largely within the range of typical oceanic cumulate values (Fig. 12). However, the absence of silica (coesite) suggests that these samples may have undergone some partial melting. In particular, the presence of coesite in eclogites has been cited as evidence for a lack of partial melting (e.g., Schulze et al. 2000). Prograde eclogite-forming reactions for plagioclase-rich compositions (i.e., B2 eclogites), as well as silica-saturated basaltic protoliths (i.e., B1 eclogites), are both expected to yield silica phases (Schulze et al. 2000). All eclogites in this study are silica free. In particular, for B1 eclogites, it is only with large modal proportions (>10 %) of silica in the bulk-rock calculations that the SiO_2 can be increased within the range of

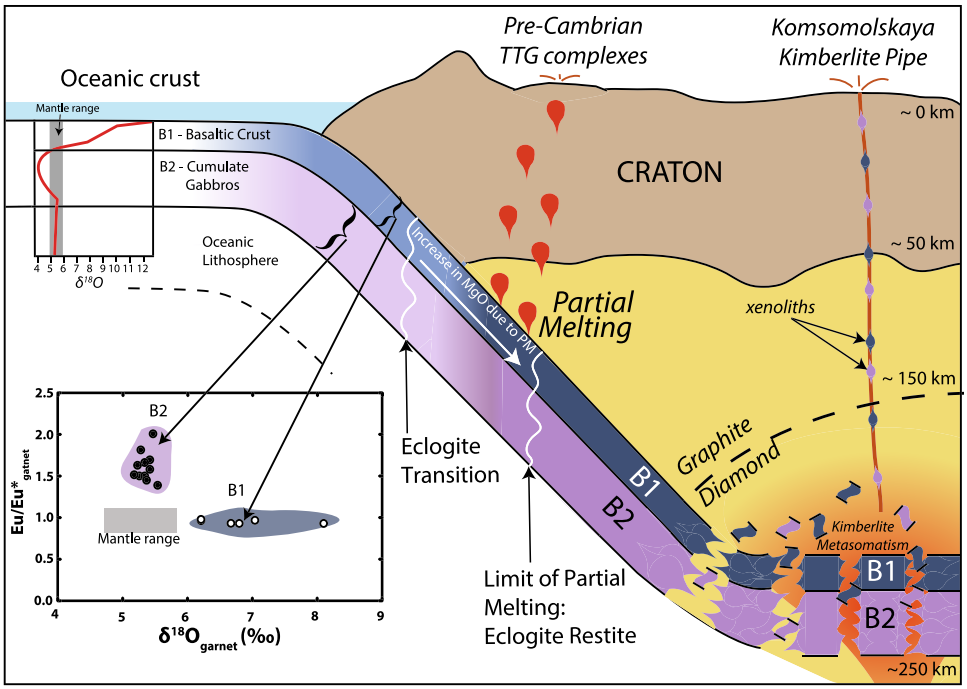

Fig. 13 Schematic diagram displaying the formation of the Komsomolskaya eclogites. The depths indicated are approximate, and the diagram is not to scale

typical basalts. It is noteworthy that Na_2O contents are all elevated in the recreated-bulk-rock values expected for a residue; however, this may simply reflect the melting of a more Na_2O-rich protolith. Despite the actual extent of melting that B2 eclogites underwent, partial melt modeling suggests that they cannot be the source of the enriched TGG-like melt, highlighting the link between basaltic sources and TGG melts.

Summary of Komsomolskaya eclogite formation

New mineral major- and trace-element data, as well as oxygen isotope ratios, from the diamondiferous eclogites of the Komsomolskaya pipe, have been used to constrain the petrogenesis of eclogites from the Siberian craton (Fig. 13). Combined trace-element and non-mantle oxygen isotope values indicate a low-pressure origin for the protoliths of these eclogites. This suite can be subdivided into two distinct groups, reflecting differing portions of the oceanic crust: (1) Group B1 eclogites represent an upper-crustal, basaltic protolith and (2) Group B2 eclogites represent lower-crustal plagioclase-rich cumulates. These lithologies were introduced into the SCLM through subduction and underplating beneath the Siberian craton during which partial melts were extracted from the slab, leading to elevated bulk-rock MgO. Partial melt models have been employed to illustrate this point, requiring large-degree melt extraction (>10 %) from a basaltic source. The compositions of the derived melts are consistent with the range of values reported for Precambrian Siberian Craton TTG complexes, further highlighting the intimate link between lithosphere formation and craton growth. Furthermore, ages reported for Siberian kimberlite-derived eclogites are consistent with a subduction origin, representing subduction events associated with craton building (Rosen et al. 2005; Pearson et al. 1995). The storage of oceanic slabs within the SCLM over time eventually leads to the break up of B1 and B2 eclogite fragments, which are subsequently metasomatized and incorporated into kimberlite melts. Overall, this suite of eclogites adds to the large body of evidence that reinforces the concept that eclogites from the Siberian SCLM represent recycled portions of Precambrian oceanic crust.

Acknowledgments The authors thank Mike Spicuzza, Allan Patchen, and Luca Fedele for their assistance with data collection. This work was funded by NSF Grants EAR-1144337 (LAT), EAR-1144559 (PHB), and EAR-0838058 (JWV). YL is currently supported at Jet Propulsion Laboratory, which is managed by California Institute of Technology, under a contract with NASA. We would like to thank Katie Smart and Ryan Ickert for constructive reviews of an earlier version of this manuscript, in addition to two anonymous reviewers for their comments and suggestions that added significantly to the revision of this manuscript.

References

Alt JC, Bach W (2006) Oxygen-isotope composition of a section of lower oceanic crust, ODP Hole 735B. Geochem Geophys Geosys 7:18

Arndt N (1983) Role of a thin, komatiite-rich oceanic crust in the Archean plate-tectonic process. Geology 11:372–375

Aulbach S, Griffin WL, Pearson NJ, O'Reilly SY, Doyle B (2007) Lithosphere formation in the central Slave Craton (Canada):

plume subcretion or lithosphere accretion? Contrib Mineral Petrol 154:409–447
Bach W, Alt JC, Niu Y, Humphris S, Erzinger J, Dick HJB (2001) The geochemical consequences of late stage low-grade alteration of the lower oceanic crust at the SW Indian ridge: results from ODP Hole 735B (Leg 176). Geochim Cosmochim Acta 65:3267–3288
Barth MG, Foley SF, Horn I (2002a) Partial melting in Archean subduction zones: constraints from experimentally determined trace element partition coefficients between eclogitic minerals and tonalitic melts under upper mantle conditions. Precambr Res 113:323–340
Barth MG, Rudnick RL, Horn I, McDonough WF, Spicuzza MJ, Valley JW, Haggerty SE (2002b) Geochemistry of xenolithic eclogites from West Africa, part 2: origins of the high MgO eclogites. Geochim Cosmochim Acta 66:4325–4345
Beard BJ, Fraracci KN, Taylor LA, Snyder GA, Clayton RA, Mayeda TK, Sobolev NV (1996) Petrography and geochemistry of eclogites from the Mir kimberlite, Yakutia, Russia. Contrib Mineral Petrol 125:293–310
Borghini G, Fumagalli P, Rampone E (2010) The stability of plagioclase in the upper mantle: subsolidus experiments on fertile and depleted lherzolite. J Petrol 51:229–254
Boyd FR (1984) Siberian geotherm based on lherzolite xenoliths from the Udachnaya kimberlite, USSR. Geology 12:528–530
Boyd FR (1989) Compositional distinction between oceanic and cratonic lithosphere. Earth Planet Sci Lett 96:15–26
Boyd FR, Pokhilenko NP, Pearson DG, Mertzman SA, Sobolev NA, Finger LW (1997) Composition of the Siberian cratonic mantle: evidence from Udachnaya peridotite xenoliths. Contrib Mineral Petrol 128:228–246
Caporuscio FA, Smyth JR (1990) Trace element crystal chemistry of mantle eclogites. Contrib Mineral Petrol 105:550–561
Carmody L, Barry PH, Shervais JW, Kluesner W, Taylor LA (2013) Oxygen-isotope in subducted oceanic crust: a new perspective from Siberian diamondiferous eclogites. Geochem Geophys Geosys. doi:10.1002/ggge.20220
Chazot G, Lowry D, Menzies M, Mattey DM (1997) Oxygen isotopic composition of hydrous and anhydrous mantle peridotites. Geochim Cosmochim Acta 61:161–169
Coleman RG, Lee ED, Beatty LB (1965) Brannock, Eclogites and eclogites: their differences and similarities. Geol Soc Am Bul 76:483–508
Davis GL, Sobolev NV, Kharkiv AD (1980) New data on the age of Yakutian kimberlites based upon U-Pb zircon method. Dokl Akad Nauk SSSR 254:175–180
Dawson JB (1984) Contrasting types of upper mantle metasomatism? In: Kimberlites II: The mantle and crust-mantle relationship proceeding of the 3rd international kimberlite conference. Elsevier, pp. 289–295
Dawson JB, Smith JV (1977) MARID (mice-amphibole-rutile-ilmenite-diopside) suite of xenoliths in kimberlite. Geochim Cosmochim Acta 41:309–323
Donskaya TV, Gladkochub DP, Pisarevsky SA, Poller U, Mazukabzov AM, Bayanova TB (2009) Discovery of Archaean crust within the Akitkan orogenic belt of the Siberian craton: new insight into its architecture and history. Precam Res 170:61–72
Doucet LS, Ionov DA, Golovin AV (2013) The origin of coarse garnet peridotite in cratonic lithosphere: new data on xenoliths from the Udachnaya kimberlite, central Siberia. Contrib Mineral Petrol 165:1225–1242
Eggins SM (1992) Petrogenesis of Hawaiian tholeiite: 1. Phase equilibria constraints. Contrib Mineral Petrol 110:387–397
Eiler JM (2001) Oxygen-isotope variations of basaltic lavas and upper mantle rocks. Rev Mineral Geochem 43:319–364
Ellis DJ, Green DH (1979) An experimental study of the effect of Ca upon garnet-clinopyroxene Fe-Mg exchange equilibria. Contrib Mineral Petrol 71:13–22
Farquhar J, Wing BA, McKeegan KD, Harris JW, Cartigny P, Thiemens MH (2002) Mass-independent sulfur of inclusions in diamond and sulfur recycling on early earth. Science 298:2369–2372
Greau Y, Huang JX, Griffin WJ, Renac C, Alard O, O'Reilly SY (2011) Type I eclogites from Roberts Victor kimberlites; products of extensive mantle metasomatism. Geochim Cosmochim Acta 75:6927–6954
Gregory RT, Taylor HP Jr (1981) An oxygen-isotope profile in a section of Cretaceous oceanic crust, Samail ophiolite, Oman: evidence for ^{18}O buffering of the oceans by deep (>5 km) seawater-hydrothermal circulation at mid-ocean ridges. J Geophys Res 86:2737–2755
Griffin WL, O'Reilly SY (2007) Cratonic lithospheric mantle: is anything subducted? Episodes 30:43–53
Griffin WL, Shee SR, Ryan CG, Win TT, Wyatt BA (1999) Harzburgite to lherzolite and back again: metasomatic processes in ultramafic xenoliths from the Wesselton kimberlite, Kimberley, South Africa. Contrib Mineral Petrol 134:232–250
Grutter HS, Gurney JJ, Menzies AH, Winter F (2004) An updated classification scheme for mantle-derived garnet, for use by diamond explorers. Lithos 77:841–857
Hart SR, Blusztain J, Dick HKB, Meyer PS, Muehlenbachs K (1999) The fingerprint of seawater circulation in a 500-meter section of ocean crust gabbros. Geochim Cosmochim Acta 63:4059–4080
Hauri EH, Shimizu N, Dieu JJ, Hart SR (1993) Evidence for hotspot-related carbonatite metasomatism in the oceanic upper mantle. Nature 365:221–227
Hill DV, Haggerty SE (1989) Petrochemistry of eclogites from the Koidu Kimberlite Complex, Sierra Leone. Contrib Mineral Petrol 103:397–422
Howarth GH, Barry PH, Pernet-Fisher JF, Pokhilenko NP, Pokhilenko LN, Bodnar RJ, Taylor LA (2014) Superplume metasomatism: evidence from Siberian mantle xenoliths. Lithos. doi:10.1016/j.lithos.2013.09.006
Huang JX, Greau Y, Griffin WL, O'Reilly SY, Pearson NJ (2012) Multi-stage origin of Roberts Victor eclogites: progressive metasomatism and its isotopic effects. Lithos 142–143:161–181
Ionov DA, Doucet LS, Ashchepkov IV (2010) Composition of the lithosphericmantle in the Siberian Craton: new constraints from fresh peridotites in the Udachnaya-East kimberlite. J Petrol 5:2177–2210
Ireland TR, Rudnick RL, Spetsius Z (1994) Trace elements in diamond inclusions from eclogites reveal link to Archean granites. Earth Planet Sci Lett 128:199–213
Irving AJ (1974) Geochemical and high pressure experimental studies of garnet pyroxenite and pyroxene granulite xenoliths from the Delegate basaltic pipe. Aust J Pet 15:1–40
Jacob DE (2004) Nature and origin of eclogite xenoliths from kimberlites. Lithos 77:295–316
Jacob DE, Foley SF (1999) Evidence for Archean ocean crust with low high field strength element signature from diamondiferous eclogite xenoliths. Lithos 48:317–336
Jacob DE, Jagoutz E, Lowry D, Mattey DM, Kudrjavtseva G (1994) Diamondiferous eclogites from Siberia: remnants of Archean oceanic crust. Geochim Cosmochim Acta 58:5191–5207
Jacob DE, Viljoen KS, Grassineau N (2009) Eclogite xenoliths from Kimberley, South Africa: a case study of mantle metasomatism in eclogites. Lithos 112:1002–1013
Jagoutz DE, Dawson JB, Hoernes S, Spettle B, Wanke H (1984) Anorthositic oceanic crust in the archean earth. 15th lunar planetary sciences conference 395

Jahn BM, Gruau G, Capdevila R, Cornichet J, Nemchin A, Pidgeon R, Rudnik VA (1998) Archean crustal evolution of the Aldan Shield, Siberia: geochemical and isotopic constraints. Precamb Res 91:333–363

Jerde EA, Taylor LA, Crozaz G, Sobolev NV, Sobolev VN (1993) Diamondiferous eclogites from Yakutia, Siberia: evidence for a diversity of protoliths. Contrib Mineral Petrol 114:189–202

Johnson KTM, Dick HJB, Shimizu N (1990) Melting in the oceanic upper mantle: ion microprobe study of diopsides in abyssal peridotites. J Geophys Res 95:2661–2678

Kamenetsky VS, Kamenetsky MB, Golovin AV, Sharygin VV, Maas R (2012) Ultrafresh salty kimberlite of the Udachnaya-East pipe (Yakutia, Russia): a petrological oddity or fortuitous discovery? Lithos 152:173–186

Kennedy CS, Kennedy GC (1976) The equilibrium boundary between graphite and diamond. J Geophys Res 81:2467–2470

Kharkiv AD, Zinchuk NN, Kryuchkov AI (1998) Diamond primary deposits of the world. Nedra Publ House Moscow (in Russian)

Krogh EJ (1998) The garnet–clinopyroxene Fe\Mg geothermometer: a reinterpretation of existing experimental data. Contrib Mineral Petrol 99:44–48

MaCandless TE, Gurney JJ (1989) Sodium in garnet and potassium in clinopyroxene: criteria for classifying mantle eclogites. In: Ross J (ed) Kimberlite and related rocks vol. 2: their mantle/crust setting, diamonds and diamond exploration. GSA Special Publication, pp. 827–832

MacGregor ID, Manton WI (1986) Roberts Victor eclogites: ancient oceanic crust. J Geophys Res 91:14063–14079

Mather KA, Pearson DG, McKenzie D, Kjarsgaard BA, Priestley K (2011) Constraints on the depth and thermal history of cratonic lithosphere from peridotite xenoliths, xenocrysts and seismology. Lithos 125:729–742

Mattey D, Lowry D, Macpherson C (1994) Oxygen-isotope composition of mantle peridotite. Earth Planet Sci Lett 128:231–241

McDonough WF, Sun S (1995) The composition of the earth. Chem Geol 120:223–253

Menzies MA, Rogers N, Tindle A, Hawkesworth CJ (1987) Metasomatic and enrichment processes in lithospheric peridotites, an effect of asthenosphere-lithosphere interaction. In: Menzies MA, Hawkesworth CJ (eds) Mantle metasomatism. Academic Press Inc., pp 313–336

Misra KC, Anand M, Taylor LA, Sobolev NV (2004) Multi-stage metasomatism of diamondiferous eclogite xenoliths from the Udachnaya kimberlite pipe, Yakutia, Siberia. Contrib Mineral Petrol 146:696–714

Muehlenbachs K, Clayton RN (1972) Oxygen-isotope geochemistry of submarine greenstones. Can J Earth Sci 9:471–478

Nisbet EG, Fowler CM (1983) Model for Archean plate tectonics. Geology 11:376–379

Pearson DG, Nixon PH (1995) Diamonds in young orogenic belts: graphitised diamonds from Beni Bousera, N. Morocco, a comparison with kimberlite-derived diamond occurrences and implications for diamond genesis and exploration. Africa Geosci Rev 3:295–316

Pearson DG, Boyd FR, Haggerty SE, Pasteris JD, Field SW, Nixon PH, Pokhilenko NP (1994) Characterization and origin of graphite in cratonic lithospheric mantle: a petrological carbon isotope and Raman spectroscopic study. Contrib Mineral Petrol 115:449–466

Pearson DG, Snyder GA, Shirey SB, Taylor LA, Carlson RW, Sobolev NV (1995) Archaean Re-Os age for Siberian eclogites and constraints on Archaean tectonics. Nature 374:711–713

Pearson DG, Canil D, Shirey SB (2003) Mantle samples included in volcanic rocks: xenoliths and diamonds. Treatise Geochem 2:171–275

Pertermann M, Hirschmann MM (2003) Partial melting experiments on a MORB-like pyroxenite between 2 and 3 GPa: constraints on the presence of pyroxenite in basalt source regions from solidus location and melting rate. J Geophys Res 108:B2

Rapp RP, Watson EB (1995) Dehydration melting of metabasalt at 8-32 kbar: implication for continental growth and crust-mantle recycling. J Petrol 36:891–931

Rehfeld T, Foley SF, Carlson RW, Lowry D, Jacob DE (2008) Contrasting types of metasomatism in dunite, wehrlite and websterite xenoliths from Kimberley, South Africa. Geochim Cosmochim Acta 72:5722–5756

Riches AJV, Liu Y, Day JMD, Spetsius ZV, Taylor LA (2010) Subducted oceanic crust as diamond hosts revealed by garnets of mantle xenoliths from Nyurbinskaya, Siberia. Lithos 120:368–378

Rosen OM, Manakov AV, Suvorov VD (2005) The collisional system in the northeastern Siberian Craton and a problem of diamond-bearing lithospheric keel. Geotectonics 39:456–479

Rudnick R (1995) Making continental crust. Nature 378:571–577

Schmickler B, Jacob DE, Foley SF (2004) Eclogite xenoliths from the Kuruman kimberlites, South Africa: geochemical fingerprinting of deep subduction and cumulate processes. Lithos 75:173–207

Schulze DJ (2003) A classification scheme for mantle-derived garnets in kimberlite: a tool for investigating the mantle and exploring for diamonds. Lithos 71:195–213

Schulze DJ, Valley JW, Spicuzza MJ (2000) Coesite eclogites from the Roberts Victor kimberlite, South Africa. Lithos 54:23–32

Smart KA, Chacko T, Stachel T, Tappe S, Stern RA, Ickert RB (2012) Eclogite formation beneath the northern Slave craton constrained by diamond inclusion: oceanic lithosphere origin without a crustal signature. Earth Planet Sci Lett 319:165–177

Snyder GA, Taylor LA, Crozaz G, Halliday AN, Beard BL, Sobolev VN, Sobolev NV (1997) The origins of Yakutian eclogite xenoliths. J Petrol 38:85–113

Sobolev NV, Lavrent'ev YG, Pokhilenko NP, Usova LV (1973) Chrome-rich garnets from kimberlites of Yakutia and their paragenesis. Contrib Mineral Petrol 40:39–52

Sobolev VN, Taylor LA, Snyder GA, Sobolev NV (1994) Diamondiferous eclogites from the Udachnaya kimberlites pipe, Yakutia. Inter Geol Rev 36:42–64

Spetsius ZV, Taylor LA (2008) Diamonds of Siberia: photographic evidence for their origin. Tranquility Base Press

Tappe S, Smart KA, Pearson DG, Steenfelt A, Simonetti A (2011) Craton formation in Late Archean subduction zones revealed by first Greenland eclogites. Geology 39:1103–1106

Taylor LA, Neal CR (1989) Eclogites with oceanic crustal and mantle signatures from the Bellsbank kimberlite, South Africa, Part I: mineralogy, petrography, and whole-rock chemistry. J Geol 97:551–567

Taylor LA, Keller RA, Snyder GA, Wang W, Carlson WD, Hauri EH, Hauri EH, Mccandless T, Kim KR, Sobolev NV, Bezborodov SM (2000) Diamonds and their mineral inclusions, and what they tell us: a detailed "pull-apart" of a diamondiferous eclogite. Inter Geol Rev 42:959–983

Turkina OM, Berezhnaya NG, Larionov AN, Lepekhina EN, Presnyakov SL, Saltykova TE (2009) Paleoarchean tonalite-trondhjemite complex in the northwestern part of the Sharyzhalgai uplift (southwestern Siberian craton): results of U-Pb and Sm-Nd study. Russ Geol Geophys 50:15–28

Valley JW (2003) Oxygen-isotopes in zircon. Rev Min Geochem 53:343–385

Valley JW, Kitchen N, Kohn MJ, Niendorf CR, Spicuzza MJ (1995) UWG-2, a garnet standard for oxygen-isotope ratios: strategies for high precision and accuracy with laser heating. Geochim Cosmochim Acta 59:5223–5231

Valley JW, Kinny PD, Schulze DJ, Spicuzza MJ (1998) Zircon megacrysts from kimberlite: oxygen-isotope variability among mantle melts. Contrib Mineral Petrol 133:1–11

Xu XS, O'Reilly SY, Griffin WL, Zhou XM (2000) Genesis of young lithospheric mantle in southeastern China: an LA-ICP-MS trace element study. J Petrol 41:111–148

Ziaja K, Foley SF, White RW, Buhre S (2013) Metamorphism and melting of picritic crust in the early Earth. Lithos. doi:10.1016/j.lithos.2013.07.001